Heliyon 9 (2023) e16490

Contents lists available at ScienceDirect

Heliyon

journal homepage: www.cell.com/heliyon

Research article

Mixed convection and activation energy impacts on MHD bioconvective flow of nanofluid with irreversibility assessment

Mujeeb ur Rahman [a], Fazal Haq [a,*], Pompei C. Darab [b], Mohammed Sallah [c,d], Shaimaa A.M. Abdelmohsen [e], Bandar M. Fadhl [f], Basim M. Makhdoum [f]

[a] Department of Mathematical Sciences, Karakoram International University, Main Campus, Gilgit, 15100, Pakistan
[b] Department of Electric Power Systems and Management, Faculty of Electrical Engineering, Technical University of Cluj-Napoca, Romania
[c] Applied Mathematical Physics Research Group, Physics Department, Mansoura University, Mansoura, 35516, Egypt
[d] Higher Institute of Engineering and Technology, New Damietta, 34517, Egypt
[e] Department of Physics, College of Science, Princess Nourah Bint Abdulrahman University, P.O. Box 84428, Riyadh, 11671, Saudi Arabia
[f] Mechanical Engineering Department, College of Engineering and Islamic Architecture, Umm Al-Qura University, P. O. Box 5555, Makkah, 21955, Saudi Arabia

ARTICLE INFO

Keywords:
Magnetic field
Entropy generation
Walter's-B nanofluid
Bioconvection
Bejan number

ABSTRACT

In this communication irreversibility minimization in bio convective Walter's-B nanofluid flow by stretching sheet is studied. Suspended nanoparticles in Walter's-B fluid are stabilized by utilizing microorganisms. Total irreversibility is obtained via thermodynamics second law. The influences of applied magnetic field, radiation, Joule heating and activation energy are accounted in momentum, temperature and concentration equations. Furthermore thermophoresis and Brownian movement impacts are also accounted in concentration and temperature expressions. The flow governing dimensional equations are altered into dimensionless ones adopting transformation procedure. Homotopy Analysis Method (HAM) code in Mathematica is implemented to get the convergent series solution. The influences of important flow variables on temperature, velocity, motile density, irreversibility, mass concentration, Bejan number and physical quantities are analyzed graphically. The obtained results revel that the velocity profile decreases for escalating magnetic parameter and Forchheimer number. Entropy generation is increased for higher Brinkman variable while Bejan number declines versus Brinkman variable. The important observations are given at the end.

1. Introduction

While modeling different manufacturing processes in engineering and industrial sector boundary layer flows of on-Newtonian fluids play vital role. Some of these processes are plastic sheets aerodynamic extrusion, applications of coating and metallic plates cooling [1–5]. Literature review revels that there are certain fluid models which have viscous and elastic properties. The Walter's-B fluid model is amongst one of these models. Walter's-B fluid model is difficult to solve as it is nonlinear in nature. Owing such properties Walter's-B fluid model has attracted researchers. Nadeem et al. [6] studied Walter's-B nanofluid flow having magnetic field influences by a convective stretchable sheet. Hayat et al. [7] disclosed heat transport in magnetized convective Walter's-B fluid flow.

* Corresponding author.
E-mail address: fazal.haq@kiu.edu.pk (F. Haq).

https://doi.org/10.1016/j.heliyon.2023.e16490
Received 7 March 2023; Received in revised form 16 May 2023; Accepted 18 May 2023
Available online 21 May 2023

Chang et al. [8] examined transport of heat in free convective viscoelastic Walter's-B fluid flow. Hayat et al. [9] explored magnetized electrically conducting 3D flow of Walter's-B fluid with solar radiation. Ramesh and Davakar [10] studied peristaltic Walter's-B fluid flow in a vertical channel.

Nanofluids are mixture of base fluids and metallic particles. Commonly used based fluids are water, ethylene glycol and oil. Nanoparticles are metals, carbon nanotubes, nitrides and metallic oxides. In industrial processes low thermal conductivity of working fluids is a barrier in effective transportation of heat. By mixing metallic tiny particles of nano-size in base fluids, the thermal conductivity of base fluids can be improved. Applications of nanofluids can be seen in computer processers, hybrid engines, air-conditioners and desert coolers. Owing such diverse applications in industrial sector and engineering nanofluids have attracted attention of researchers in the current decadeAlsharif et al. [11] scrutinized the characteristics of hybrid second grade nanomaterial by upright microchannel with Cattaneo model for heat transportation. Gowda et al. [12] explored the features of rotating flow of Casson–Maxwell nanoliquid accounting Cattaneo–Christov diffusion concept. Impact of radiation and dual phase lag conduction through optically participating spherical enclosure is reported by Mukherjee and Mondal [13]. Ziaei et al. [14] explored MHD nanofluid flow by permeable stretching surface. Consequences of porosity and activation energy in flow of hybrid nanofluid by curved stretched is investigated by Kumar et al. [15].

When moving gyrotactic microorganisms are added to the base fluid bio convection happens. The microorganisms are denser than base fluids. Due to their self-propelled nature the microorganisms move vertically upward as a result mass concentration at upper surface of fluid upsurges. The upper surface becomes unstable and microorganisms fall down to produce bio convection in the fluid. The status quo is maintained by swimming of microorganisms back to upper surface. Applications of microorganisms can be seen in enzyme biosensor, medical engineering biomedicine and bacteria powered micro mixers like biological polymer synthesis, fuel cell technology, fertilizers, sustainable fuel cell technologies and bioreactors. Khan et al. [16] disclosed bio convective flow with characteristics of mass and heat and transfer in a wavy cone. Xu and Pop [17] investigated bio convective flow in a horizontal channel. Tham et al. [18] reported nanoliquid flow having mixed convection and microorganisms embedded in porous medium moving towards a solid sphere. Combine effects of Darcy-Forchheimer and stratification in magnetized Williamson nanoliquid flow by a stretched cylinder is disclosed by Ali et al. [19]. Aziz et al. [20] analyzed bio convective nanoliquid flow with mixed convection. Sensitivity analysis for bioconvective flow of non-Newtonian Casson nanomaterial with activation energy and thermal radiation is reported by Sarkar et al. [21]. Akbar and Khan [22] analyzed magnetized flow of nanofluid having gyrotactic microorganisms. Mutuku and Makinde [23] studied hydro-magnetic nanoliquid flow having gyrotactic microorganisms by permeable vertical plate. Kuznettsov and Avramenko [24] discovered the stability of microorganisms and nanoparticles in dilute suspension. Assessment of irreversibility in stratified bioconvective flow of Cross fluid which contains oxytactic microorganisms and solid tiny particles is presented by Ali et al. [25]. Physical aspects of chemical reaction and thermal radiation in magnetized flow of non-Newtonian material by stretched sheet are examined by Gowda et al. [26].

The measure of system disorder or unobtainable energy in a dynamical closed system is called entropy. According to thermodynamics second law, in ideal cases for irreversible processes total irreversibility increases always while for reversible processes or steady state (equilibrium) irreversibility entropy remains constant. Chemical reaction, Joule heating and diffusion are a few examples of irreversible processes. By minimizing the irreversibility rate thermal system's efficiency can be enhanced. Application of irreversibility can be seen in various systems like nuclear reactors, chillers, air separators, helical coils, gas turbines and fuel cells. Bejan [27] has done pioneer works on entropy generation. Khan et al. [28] discovered irreversibility in Sisko nanoliquid flow with heat source/sink. Ramesh et al. [29] examined irreversibility in hybrid nanofluid flow in a rotating frame with radiation and magnetic field effects. Hayat et al. [30] disclosed minimization of irreversibility in chemically reactive MHD nanomaterial flow with radiation and activation energy. Gul et al. [31] discovered irreversibility in viscoelastic Poiseuille flow. Xie and Jian [32] analyzed irreversibility in MHD nanofluid flow in micro-parallel channels. Khan et al. [33] discussed entropy in viscous nanofluid flow with forced convection. Huminic and Huminic [34] disclosed irreversibility in hybrid nanofluid flow in a flattened tube. Hayat et al. [35] explored irreversibility in flow of a nanoliquid by rotating system. Nouri et al. [36] studied irreversibility in a nanoliquid flow having spherical heat source. Vatanmakan et al. [37] reported irreversibility in steam flow with volumetric heating and turbine blades. Irreversibility examination in dissipative viscous Newtonian fluid moving in a porous microchannel among two passionate parallel plates is investigated by Gaikwad et al. [38]. Sarma et al. [39] reported the consequences of electrical forcing and applied pressure gradient in water-alumina nanofluid flow with irreversibility analysis.

This communication aims to investigate the irreversibility in bioconvective flow of Walter's-B nanofluid. The effects of magnetic field, porosity of surface, Darcy Forchheimer, thermal radiation, heat generation are considered in modeling of Walter's-B nanofluid. Furthermore activation and chemical reaction aspects are accounted. The literature cited above inspires that such investigation is not reported till now. Thus this study aims to fill this gape. The obtained flow model is solved HAM code in Mathematica package. Impact of different flow controlling parameters on velocity, temperature, concentration, irreversibility rate, Bejan number and physical quantities are studied graphically. Some applications related to the current studies are mentioned in the studies like Cattaneo-Christov heat flux [40], heterogeneous sedimentary media [41], radiative time dependent flow [42], nanosheets [43], porous fiber [44], radiation process [45], modeling [46] and nanofluidics and magnetic effects [47–49]..

2. Problem formulation

Here 2D incompressible steady magnetized Walter's- B nanofluid flow by stretchable porous sheet holding gyrotactic microorganisms is addressed. Velocity of stretching sheet is $u_w = ax$, where a is a positive constant (stretching rate). For small Reynolds's number values, induced magnetic field is supposed as negligible. Schematic flow diagram is depicted in Fig. 1. Boundary layer theory is

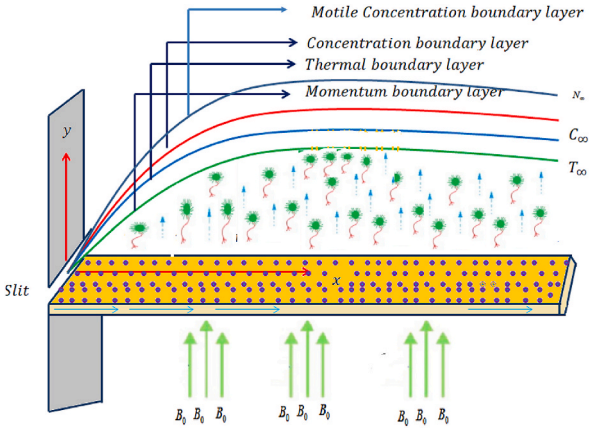

Fig. 1. Schematic flow diagram.

considered during the whole treatment of modeling. Following assumptions are considered in modeling and analysis:

- Darcy-Forchheimer and permeability impacts are taken in the modeling of momentum expression.
- Energy relation is modeled by accounting influences of heat generation, dissipation and radiation.
- Gyrotactic type microorganisms are added to stabilize the nono-sized tiny particles with in Walter's- B fluid.
- In concentration equation activation energy effect is considered.
- Thermophoresis and Brownian movement effects are accounted.
- Effects of Joule heating are considered.

The PDEs for the considered flow on the basis of above suppositions are as follows [6–8,39]:

$$\frac{\partial u}{\partial x}+\frac{\partial v}{\partial y}=0, \tag{1}$$

$$u\frac{\partial u}{\partial x}+v\frac{\partial u}{\partial y}=\frac{\nu}{\rho}\frac{\partial^2 u}{\partial y^2}-\frac{k_0}{\rho}\left(u\frac{\partial^3 u}{\partial x\partial y^2}+v\frac{\partial^3 u}{\partial y^3}-\frac{\partial u}{\partial y}\frac{\partial^2 u}{\partial x\partial y}+\frac{\partial u}{\partial x}\frac{\partial^2 u}{\partial y^2}\right)-\frac{\sigma B_0^2}{\rho}u-\frac{\mu}{\rho k_p}u-F_e u^2, \tag{2}$$

$$\begin{aligned}u\frac{\partial T}{\partial x}+v\frac{\partial T}{\partial y}=&\frac{k}{\rho C_p}\frac{\partial^2 T}{\partial y^2}+\tau\left[D_B\frac{\partial T}{\partial y}\frac{\partial C}{\partial y}+\frac{D_T}{T_\infty}\left(\frac{\partial T}{\partial y}\right)^2\right]-\frac{16\sigma^* T_\infty^3}{3k^*\rho C_p}\frac{\partial T}{\partial y}+\frac{Q_0}{\rho C_p}(T-T_\infty)\\&-\frac{\sigma B_0^2}{\rho C_p}u^2+\frac{\mu}{\rho C_p}\left(\frac{\partial u}{\partial y}\right)^2-\frac{k_0}{\rho C_p}\left[\frac{\partial u}{\partial y}\frac{\partial}{\partial y}\left(u\frac{\partial u}{\partial x}+v\frac{\partial u}{\partial y}\right)\right],\end{aligned} \tag{3}$$

$$u\frac{\partial C}{\partial x}+v\frac{\partial C}{\partial y}=\frac{D_T}{T_\infty}\left(\frac{\partial T}{\partial y}\right)^2+D_B\frac{\partial^2 C}{\partial y^2}-K_r^2(C-C_\infty)\left[\frac{T}{T_\infty}\right]^n\exp\left[\frac{-E_a}{\kappa T}\right], \tag{4}$$

$$u\frac{\partial N}{\partial x}+v\frac{\partial N}{\partial y}=D_m\frac{\partial^2 N}{\partial y^2}-\frac{bW_c}{(C_w-C_\infty)}\left[\frac{\partial}{\partial y}\left(N\frac{\partial C}{\partial y}\right)\right], \tag{5}$$

with

$$\left.\begin{aligned}&u=u_w(x)=ax, v=0, T=T_w, N=N_w, C=C_w \text{ at } y=0\\&u\to 0, T\to T_\infty, N\to N_\infty, C\to C_\infty \text{ at } y\to\infty.\end{aligned}\right\} \tag{6}$$

Considering

$$\left.\begin{aligned}&u=axf'(\eta), v=-\sqrt{a\nu}f(\eta), \eta=y\sqrt{\frac{a}{\nu}},\\&\theta(\eta)=\frac{T-T_\infty}{T_w-T_\infty}, \varphi(\eta)=\frac{C-C_\infty}{C_w-C_\infty}, \xi(\eta)=\frac{N-N_\infty}{N_w-N_\infty}.\end{aligned}\right\} \tag{7}$$

Using (7), equations (1)–(5) take the form (8-12), while non dimensional variables are defined in (13):

$$ff''-f'^2+f'''+\beta_1\left(ff^{(iv)}+f''^2-2f'f'''\right)-(\lambda+M)f'-Frf'^2=0, \tag{8}$$

$$\left(1+\frac{4}{3}R\right)\theta''+\Pr Nb\theta'\varphi'+\Pr Nt\theta'^2+\Pr Q\theta+\Pr MEcf'^2+\Pr Ecf''^2-\Pr\beta_1 Ec\left(f'ff''^2-f'f''f'''\right)+\Pr f\theta'=0,\Big\} \tag{9}$$

$$\varphi''+\frac{Nt}{Nb}\theta''-Sc\gamma\varphi(1+\delta_1\theta)^n\left[\frac{-E_1}{1+\delta_1\theta}\right]+Scf\varphi'=0, \tag{10}$$

$$\xi''+Lbf\xi'-Pe[\varphi'\xi'+\Omega\varphi''+\xi\varphi''=0,] \tag{11}$$

with

$$\left.\begin{array}{l} f(0)=0,f'(0)=1,\theta(0)=1,\xi(0)=1,\varphi(0)=1 \quad \text{at } \eta=0 \\ f'(\infty)\to 0,\theta(\infty)\to 0,\xi(\infty)\to 0,\varphi(\infty)\to 0 \ \text{ as } \eta\to\infty. \end{array}\right\} \tag{12}$$

here

$$\left.\begin{array}{l} \beta_1=\dfrac{ak_o}{\mu},Fr=\dfrac{C_b}{\sqrt{k}},M=\sqrt{\dfrac{\sigma B_0^2}{\rho a}},\lambda=\dfrac{\nu}{ak_p},\Pr=\dfrac{\mu c_p}{k},Lb=\dfrac{\nu}{D_m}, \\ R=\dfrac{4\sigma^* T_\infty^3}{3k^* k},Nb=\dfrac{\tau D_B(C_w-C_\infty)}{\upsilon},Nt=\dfrac{\tau D_T(T_w-T_\infty)}{T_\infty\upsilon},Ec=\dfrac{u_w^2}{C_p(T_w-T_\infty)},Pe=\dfrac{bW_c}{D_m} \\ Q=\dfrac{Q_0}{\rho C_p a},\gamma=\dfrac{k_r^2}{a},Sc=\dfrac{\nu}{D_B},\delta_1=\dfrac{T_w-T_\infty}{T_\infty},E_1=\dfrac{E_a}{\kappa T_\infty},\Omega=\dfrac{N_\infty}{N_w-N_\infty}, \end{array}\right\} \tag{13}$$

2.1. Physical quantities

Physical quantities are as follows

$$\left.\begin{array}{l} Cf_x=\dfrac{-\tau_w}{\rho u_w^2},Nu_x=\dfrac{xq_w}{k(T_w-T_\infty)}, \\ Sh_x=\dfrac{xq_m}{k(C_w-C_\infty)},Nn_x=\dfrac{xq_n}{D_m(N_w-N_\infty)} \end{array}\right\} \tag{14}$$

where wall shear stress (τ_w), heat flux at wall (q_w) and wall mass flux (q_m) are as follows:

$$\tau_w=\mu\left(\frac{\partial u}{\partial y}\right)_{y=0}-k_o\left(u\frac{\partial^2 u}{\partial x\partial y}-2\frac{\partial u}{\partial x}\frac{\partial u}{\partial y}\right)_{y=0},q_n=-D_n\left(\frac{\partial N}{\partial y}\right)_{y=0}$$

$$q_w=-k\left(1+\frac{16\sigma^* T_\infty^3}{3k^* k}\right)\left(\frac{\partial T}{\partial y}\right)_{y=0},q_m=-D_B\left(\frac{\partial C}{\partial y}\right)_{y=0}.$$

Final versions of (14) is given in (15)

$$\left.\begin{array}{l} Cf_x(\mathrm{Re}_x)^{\frac{1}{2}}=f''(0)\ [1+\beta_1 f'(0)], \\ Nu_x(\mathrm{Re}_x)^{-\frac{1}{2}}=-\left[1+\dfrac{4}{3}R(1+\delta_1(0))^3\right]\theta'(0), \\ Sh_x(\mathrm{Re}_x)^{-\frac{1}{2}}=-\varphi'(0),Nn_x(\mathrm{Re}_x)^{-\frac{1}{2}}=-\xi'(0). \end{array}\right\} \tag{15}$$

where $\mathrm{Re}_x\left(=\frac{ax^2}{\nu}\right)$ is local Reynold's number.

2.2. Entropy generation

The irreversibility rate is:

$$\left.\begin{array}{l} E_G=\dfrac{k}{T_\infty^2}\left[1+\dfrac{4}{3}R\right]\left(\dfrac{\partial T}{\partial y}\right)^2+\dfrac{\sigma B_0^2}{T_\infty}u^2+\dfrac{\mu}{T_\infty k_p}u^2+\dfrac{\mu}{T_\infty}\mu\left(\dfrac{\partial u}{\partial y}\right)^2-k_0\dfrac{\partial u}{\partial y}\dfrac{\partial}{\partial y}\left\{u\dfrac{\partial u}{\partial x}+v\dfrac{\partial u}{\partial y}\right\}+\dfrac{RD}{C_\infty}\left(\dfrac{\partial C}{\partial y}\right)^2+ \\ \dfrac{RD}{T_\infty}\left(\dfrac{\partial T}{\partial y}\right)\left(\dfrac{\partial C}{\partial y}\right)+\dfrac{RD}{N_\infty}\left(\dfrac{\partial N}{\partial y}\right)^2+\dfrac{RD}{T_\infty}\left(\dfrac{\partial T}{\partial y}\right)\left(\dfrac{\partial N}{\partial y}\right), \end{array}\right\} \tag{16}$$

dimensionless form of irreversibility rate is

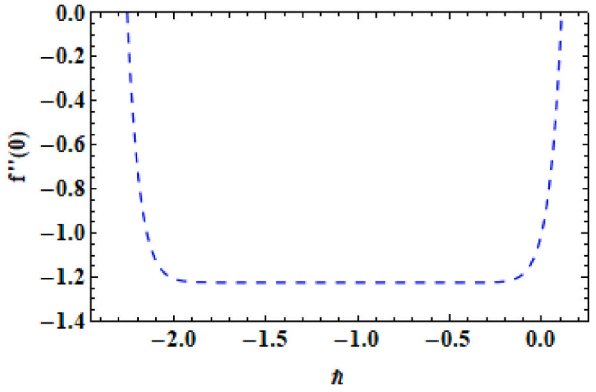

Fig. 2. $\hbar$ curve for $f''(0)$.

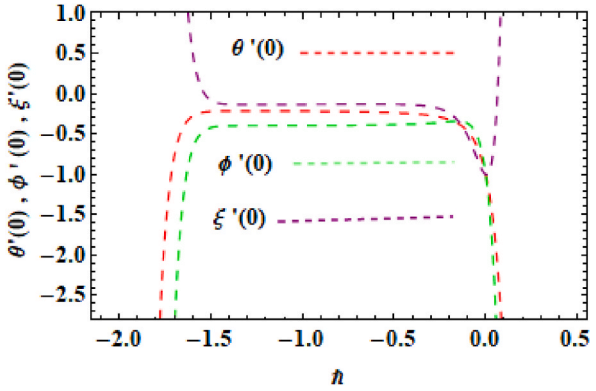

Fig. 3. $\hbar$ curve for $\theta'(0), \varphi'(0)$ and $\xi'(0)$.

$$S_G = \frac{E_G}{E_{G_0}} = \left(1+\frac{4}{3}R\right)\delta_1\theta'^2 + MB_r f'^2 + B_r\lambda f'^2 + B_r f''^2 - \beta B_r\left(f'^2 f''^2 - ff''f'''\right) + L\frac{\alpha_2}{\delta_1}\varphi'^2 + L\theta'\varphi' + L_1\frac{\alpha_3}{\delta_1}\xi'^2 + L_1\xi'\varphi'. \Big\} \tag{17}$$

Non-dimensional variables appeared in (16 & 17) are defined as entropy generation rate $S_G\left(=\frac{E_G T_\infty \nu}{ak(T_w-T_\infty)}\right)$, $E_{G_0}\left(=\frac{k(T_w-T_\infty)}{T_\infty}\left(\frac{a}{\nu}\right)\right)$ is characteristic entropy generation rate, $B_r\left(=\frac{\mu a^2 x^2}{k(T_w-T_\infty)}\right)$ Brink man number, $L\left(=\frac{RD_B(C_w-C_\infty)}{k}\right)$ diffusion parameter, $\alpha_2\left(=\frac{C_w-C_\infty}{C_\infty}\right)$ difference ratio parameter for concentration, $\alpha_3\left(=\frac{N_w-N_\infty}{N_\infty}\right)$ difference ratio variable for motile density and $L_1\left(=\frac{RD_B(N_w-N_\infty)}{k}\right)$ diffusion parameter for motile density.

3. Solution procedure

Here via HAM code in Mathematica software solution is constructed. The initial guesses for the chosen problem are:

$$f_0(\eta) = 1 - e^{-\eta}, \theta_0(\eta) = e^{-\eta},$$
$$\varphi_0(\eta) = e^{-\eta}, \xi_0(\eta) = e^{-\eta},$$

linear operators are:

$$L_f = f''' - f', L_\theta = \theta'' - \theta,$$
$$L_\varphi = \varphi'' - \varphi, L_\xi = \xi'' - \xi,$$

with

$$L_f\left(c_1 + c_2 e^{\eta} + c_3 e^{-\eta}, L_\theta(c_4 e^{\eta} + c_5 e^{-\eta}\right),$$
$$L_\varphi(c_6 e^{\eta} + c_7 e^{-\eta}), L_\xi(c_8 e^{\eta} + c_9 e^{-\eta}),$$

Table 1
Numerical experiments for $f''(0)$, $\theta'(0)$, $\varphi'(0)$ and $\xi'(0)$.

Iterations	$f''(0)$	$\theta'(0)$	$\varphi'(0)$	$\xi'(0)$
1	1.100	0.597	0.368	1.143
5	1.133	0.413	0.759	0.666
10	1.132	0.373	0.802	0.751
15	1.132	0.359	0.815	0.782
20	1.131	0.353	0.820	0.793
25	1.131	0.350	0.820	0.7991
30	1.131	0.350	0.820	0.7991

Table 2
Comparison of results for gradient of temperature.

Pr	Wang [50]	Khan and Pop [51]	Recent result
0.07	0.0656	0.0656	0.0657
0.20	0.1691	0.1691	0.1692
0.70	0.4539	0.4539	0.4539
2.00	0.9114	0.9114	0.9115
7.00	1.8954	1.8954	1.8955
20.00	3.3539	3.3539	3.3539

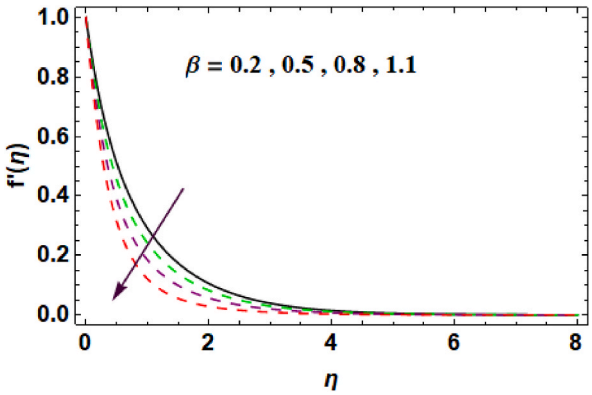

Fig. 4. $f'(\eta)$ through β.

where $c_i (i = 1 - 9)$ stands for arbitrary constants.

3.1. Convergence analysis

In homotopy approach the region of convergence of series solution is controlled by auxiliary variables $\hbar_f, \hbar_\theta, \hbar_\varphi$ and $\hbar_\xi$. In Figs. 2.1 and 2.2 $\hbar$ curves for temperature, velocity, motile density and concentration are plotted. The suitable ranges for these variables are $-2.0 \leq \hbar_f \leq 0.0$, $-1.8 \leq \hbar_\theta \leq 0.1$, $-1.7 \leq \hbar_\varphi \leq 0.1$ and $-1.6 \leq \hbar_\xi \leq 0.0$. The convergence is further justified numerically through Table 1. From Table 1 and it is observed that 20th, 15th, 20th and 10th order of iterations are enough for convergence of $f''(0)$, $\theta'(0)$, $\varphi'(0)$, and $\xi'(0)$. Accuracy of current analytical scheme is confirmed in Table 2. In Table 2 gradient of temperature is computed for various estimations of Pr whereas all other sundry variables are set to be zero with Wang [50] and Khan and Pop [51]. An excellent agreement is observed.

4. Results and discussions

HAM code is implemented to find the solution of dimensionless system of ODEs. Pertinent flow parameters impact on velocity $(f'(\eta))$, concentration $(\varphi(\eta))$, temperature $(\theta(\eta))$, and motile density $(\xi(\eta))$, physical quantities, irreversibility and Bejan number are analyzed in this section. Graphical results are acquired takin specific ranges of physical parameters like $0.1 \leq \beta \leq 1.1$, $0.5 \leq \lambda \leq 2.0$, $0.3 \leq Fr \leq 1.8$, $0.1 \leq R \leq 1.8$, $0.1 \leq Nb \leq 1.8$, $0.1 \leq Nt \leq 1.8$, $0.3 \leq Ec \leq 1.5$, $0.4 \leq Q \leq 1.6$, $0.3 \leq Sc \leq 0.6$, $0.3 \leq E_1 \leq 0.9$, $0.4 \leq Lb \leq 1.0$, $0.3 \leq Pe \leq 0.9$, $0.3 \leq \Omega \leq 2.1$, $0.4 \leq Br \leq 2.0$, $0.1 \leq L \leq 1.7$, $0.2 \leq L_1 \leq 1.0$.

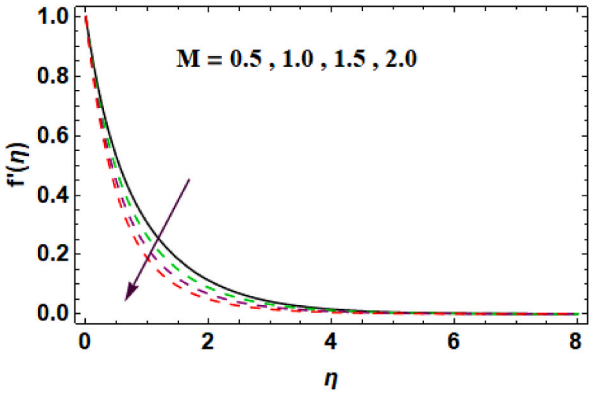

Fig. 5. $f^{'}(\eta)$ through M.

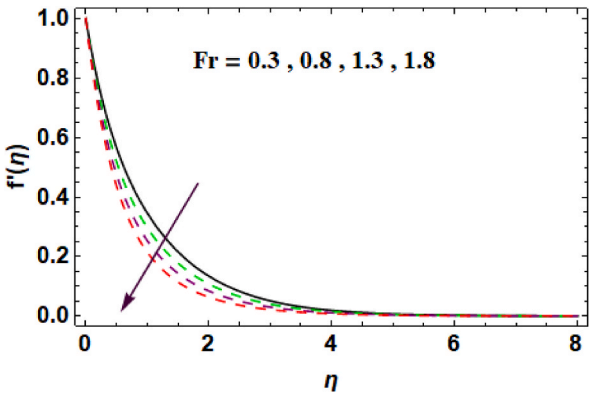

Fig. 6. $f^{'}(\eta)$ via Fr.

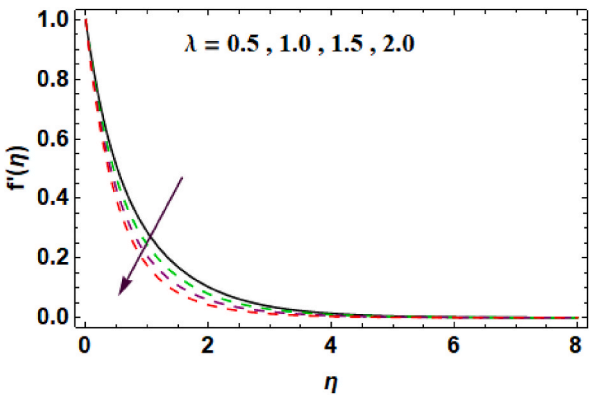

Fig. 7. $f^{'}(\eta)$ via λ.

4.1. Velocity profiles

Figs. $(4-7)$ are plotted to check the impacts of β, M, Fr and λ on $f^{'}(\eta)$. Fig. 4 portrays influence of β on $f^{'}(\eta)$. Velocity diminishes for higher β values. In fact higher β enhances viscoelastic effects in the fluid and thus fluid velocity decays. Fig. 5 gives impact of M on $f^{'}(\eta)$. Clearly $f^{'}(\eta)$ decreases for escalating values of M. For higher values of M resistive force which opposes motion of fluid increases so $f^{'}(\eta)$ decreases. Fig. 6 shows that for raising values of Fr velocity profile decreases. Since higher Fr corresponds to more drag force, which opposes the flow and thus $f^{'}(\eta)$ decays. Fig. 7 portrays that higher λ retards $f^{'}(\eta)$. Physically for higher porosity variable values size of pours upsurges as a result permeability increases so velocity decreases.

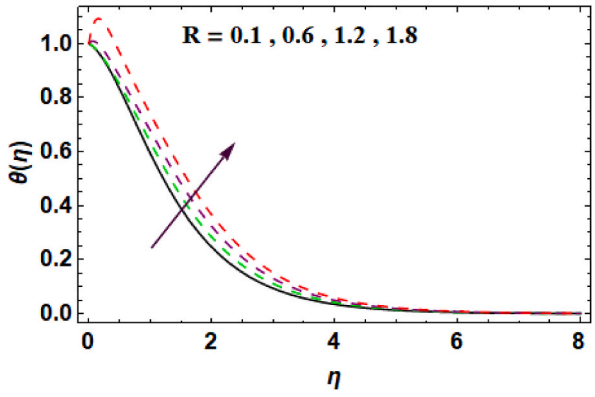

Fig. 8. $\theta(\eta)$ through R.

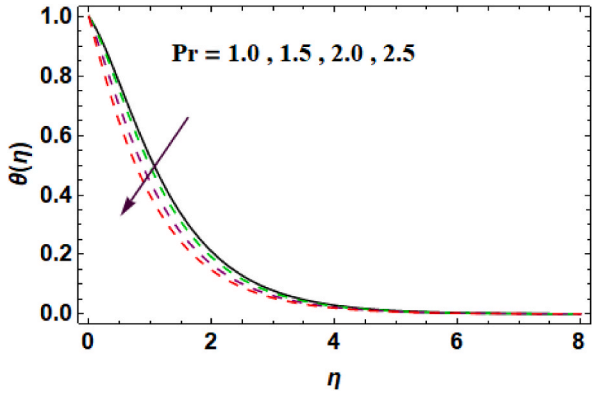

Fig. 9. $\theta(\eta)$ through Pr.

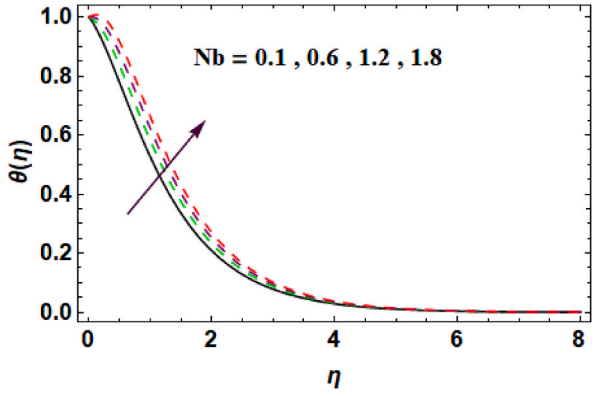

Fig. 10. $\theta(\eta)$ versus Nb.

4.2. *Temperature profiles*

Here influences of R, Pr, Nb, Nt, M, Ec and Q on $\theta(\eta)$ are expressed in Figs. $(8-14)$. Impact of R on $\theta(\eta)$ is given in Fig. 8. For raising R the temperature upsurges. For higher R surface heat flux boosts as a results temperature increases. Pr impact on $\theta(\eta)$ is portrayed in Fig. 9 Due to enlargement in Pr values $\theta(\eta)$ decreases. Physically for larger Pr, thermal diffusivity decreases therefore $\theta(\eta)$ decays. Fig. 10 gives effect of Nb on $\theta(\eta)$. For greater Nb values $\theta(\eta)$ escalates. For larger Nb fluid particles random movement increases so more collision among fluid particles occurs therefore more heat produces thus fluid temperature increases. Fig. 11 is plotted to check the effect of Nt on $\theta(\eta)$. For raising Nt values fluid temperature upturns. For higher Nt more fluid particles are shifted from heated surface to cold region so $\theta(\eta)$ rises. Fig. 12 shows M effect on $\theta(\eta)$, here thermal field boosts. Physically magnetic field produces more resistive

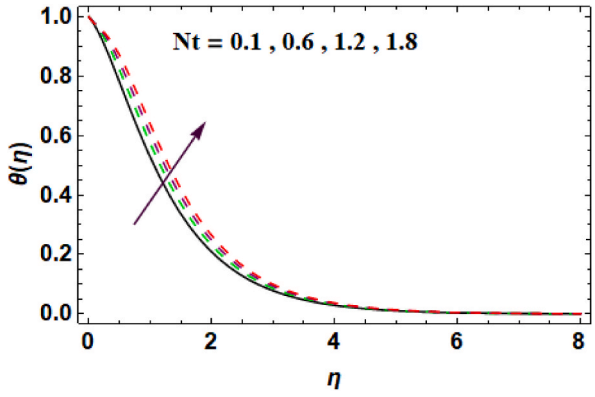

Fig. 11. $\theta(\eta)$ versus *Nt*.

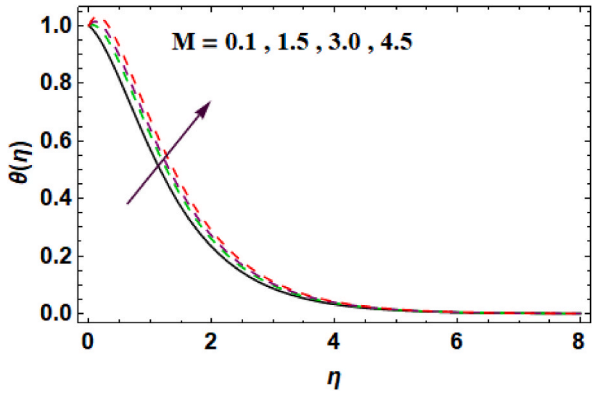

Fig. 12. $\theta(\eta)$ via *M*.

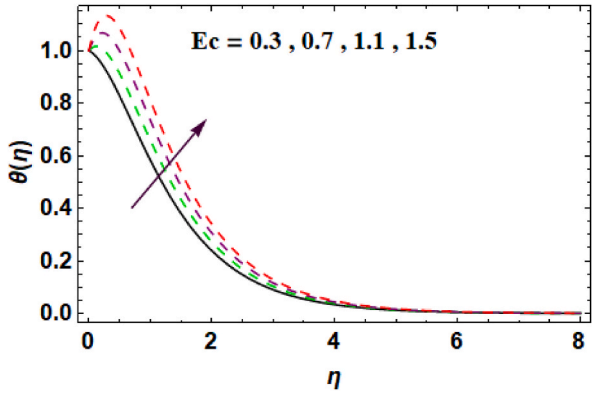

Fig. 13. $\theta(\eta)$ versus *Ec*.

force in opposite direction of flow thus more heat produces so $\theta(\eta)$ increases. In Fig. 13 Eckert number influence on $\theta(\eta)$ is shown. For escalating *Ec* values $\theta(\eta)$ upsurges. Physically fluid particles kinetic energy increases due to which internal energy of system enhances thus temperature upsurges. Fig. 14 gives effect of *Q* on $\theta(\eta)$. For larger *Q* values $\theta(\eta)$ upturns. Since improvement in heat generation variable supplies more heat to the system due to which thermal field boosts.

4.3. Concentration

Figs. $(15-19)$ show influences of *Nb*, *Nt*, γ, *Sc*, and E_1 on $\varphi(\eta)$. Fig. 15 is devoted to express impact of *Nb* on $\varphi(\eta)$. Concentration decreases for higher *Nb*. Physically, for higher *Nb* values collision between particles of liquid increases therefore more heat produces

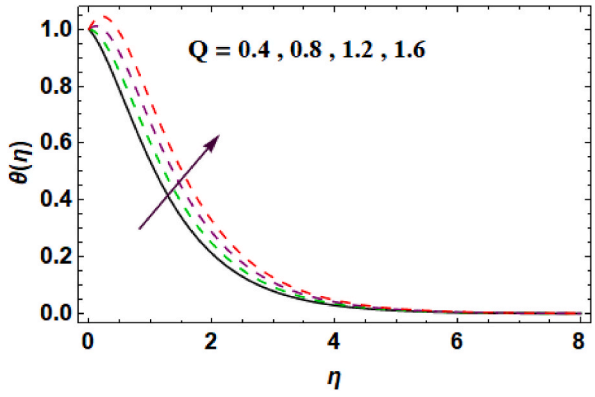

Fig. 14. Q impact on $\theta(\eta)$.

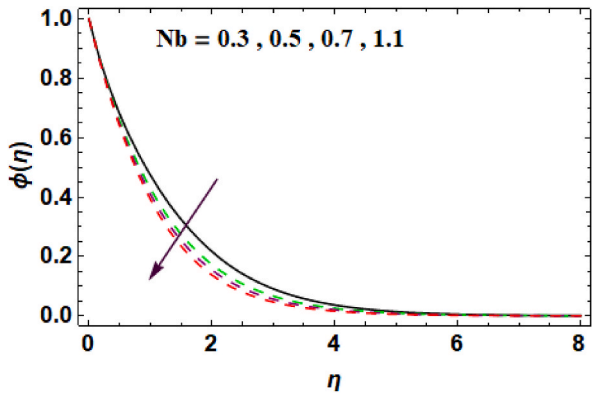

Fig. 15. *Nb* impact on $\varphi(\eta)$.

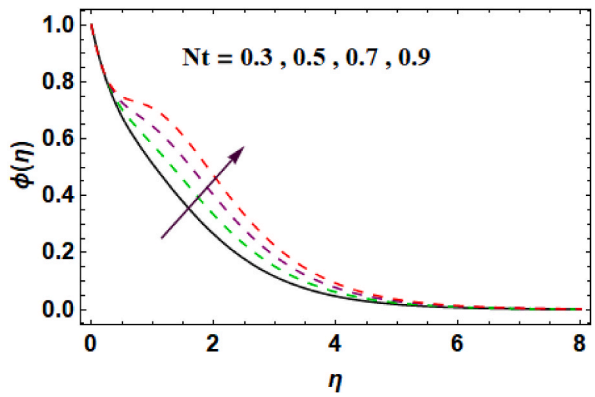

Fig. 16. *Nt* impact on $\varphi(\eta)$.

due to which temperature increases and $\varphi(\eta)$ decreases. Fig. 16 gives influence of *Nt* on $\varphi(\eta)$. Concentration rises for higher *Nt*. For raising *Nt* values thermophoretic force upsurges which shifts nanoparticles from higher to lower temperature region therefore $\varphi(\eta)$ upturns. Fig. 17 represents influence of γ on $\varphi(\eta)$. Concentration decreases for higher γ. For higher chemical reaction variable the destructive chemical reaction increases so $\varphi(\eta)$ decreases. Fig. 18 depicts *Sc* impact on $\varphi(\eta)$. Concentration decreases for upturn in *Sc* values. For larger *Sc* molecular diffusivity decreases which corresponds to smaller $\varphi(\eta)$. Fig. 19 gives impact of E_1 on $\varphi(\eta)$. Concentration upturns for higher E_1. In fact modified Arrhenius function enhances due to which rate of destructive reaction decays, consequently $\varphi(\eta)$ enhances.

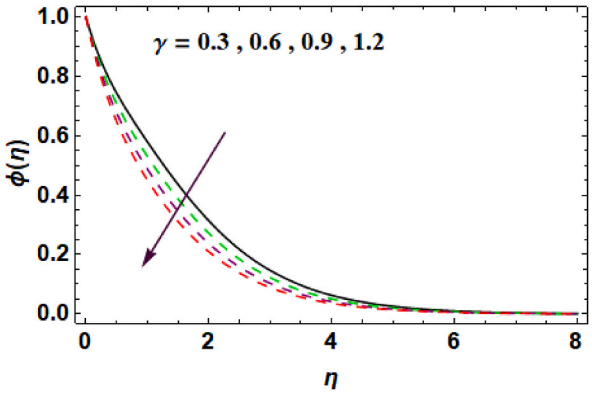

Fig. 17. $\varphi(\eta)$ through γ.

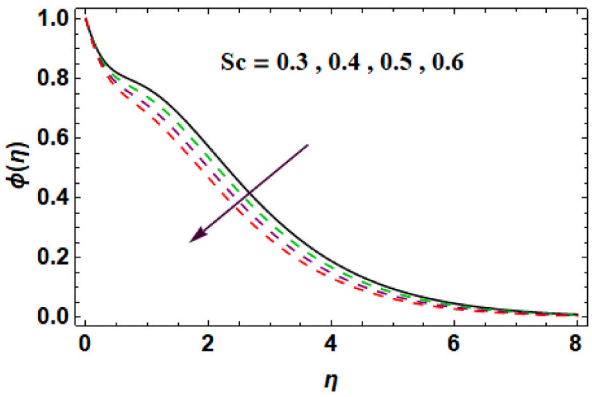

Fig. 18. $\varphi(\eta)$ through *Sc*.

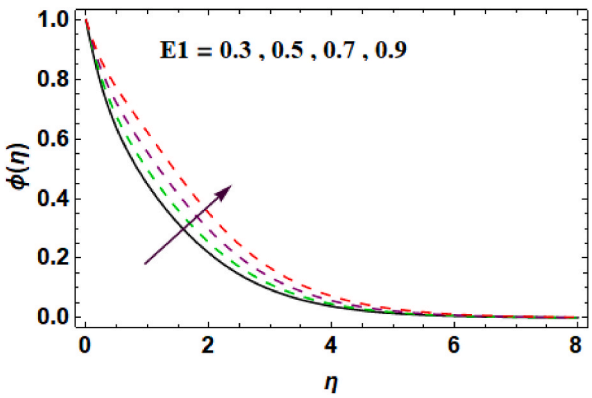

Fig. 19. $\varphi(\eta)$ versus E_1.

4.4. Motile density

Figs. $(20-22)$ are drawn to check the impacts of *Lb*, *Pe* and Ω on $\xi(\eta)$. Fig. 20 displays influence of *Lb* on $\zeta(\eta)$. Motile density decreases for higher *Lb*. Due to upturn in *Lb* microorganisms diffusivity in fluid decreases, consequently $\xi(\eta)$ declines. Fig. 21 shows impact of *Pe* on $\xi(\eta)$. Motile density decreases versus higher *Pe*. For greater *Pe* microorganisms diffusivity decays, thus $\xi(\eta)$ and related layer thickness decreased. Effect of Ω on $\xi(\eta)$ is checked in Fig. 22. It is perceived that for higher Ω the motile density of microorganisms decreases. For higher Ω concentration of microorganisms in ambient fluid escalates so motile density decays.

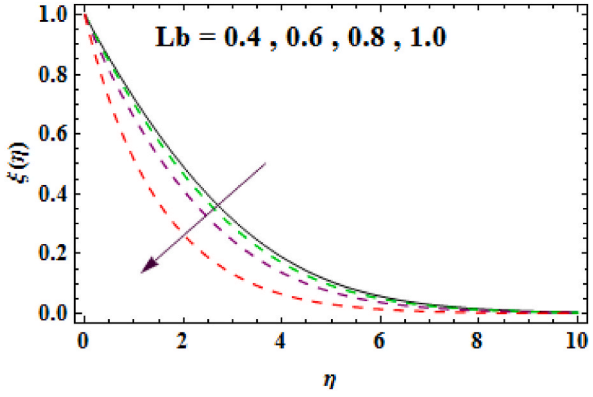

Fig. 20. *Lb* impact on $\xi(\eta)$.

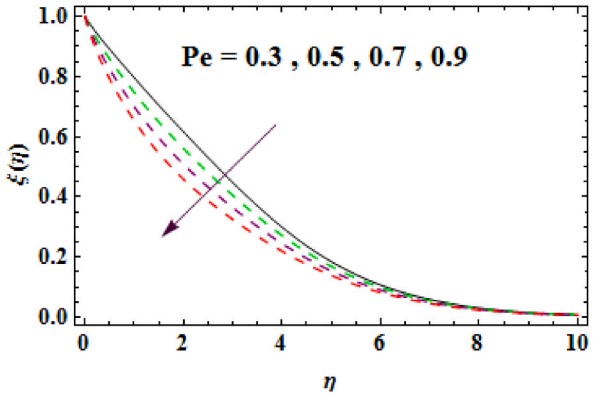

Fig. 21. *Pe* impact on $\xi(\eta)$.

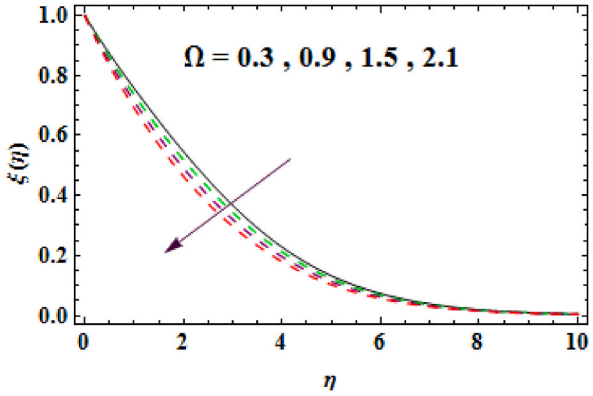

Fig. 22. Ω impact on $\xi(\eta)$.

4.5. *Engineering quantities*

This section is devoted to discuss the physical quantities like, drag force of surface $\left(Cf_x(\mathrm{Re}_x)^{\frac{1}{2}}\right)$, heat transfer rate $\left(Nu_x(\mathrm{Re}_x)^{-\frac{1}{2}}\right)$, local density number $\left(Nn_x(\mathrm{Re}_x)^{-\frac{1}{2}}\right)$ and Sherwood number $\left(Sh_x(\mathrm{Re}_x)^{-\frac{1}{2}}\right)$ versus dominant flow parameters. In Fig. 23 behavior of $Cf_x(\mathrm{Re}_x)^{\frac{1}{2}}$ is checked for higher values of *Fr* and β. Clearly for upturn in *Fr* and β, $Cf_x(\mathrm{Re}_x)^{\frac{1}{2}}$ upsurges. For increasing values of β the magnitude of drag force escalates therefore $Cf_x(\mathrm{Re}_x)^{\frac{1}{2}}$ upturns. Heat transfer rate versus growing values of Pr and *Nt* is analyzed in Fig. 24. For raising values of Pr and *Nt* heat transfer rate decreases. Conduct of $Sh_x(\mathrm{Re}_x)^{-\frac{1}{2}}$ against higher *Sc* and *Nt* is discussed via

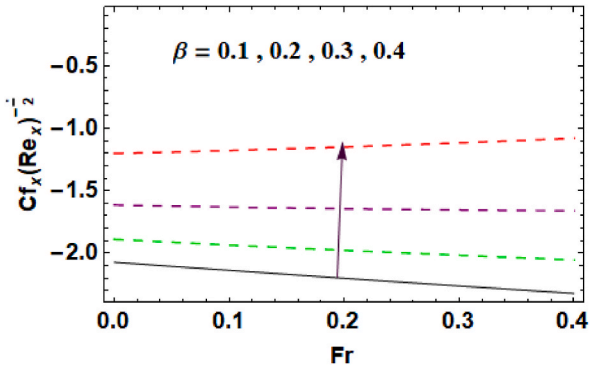

Fig. 23. $Cf_x(\mathrm{Re}_x)^{\frac{1}{2}}$ versus β and Fr.

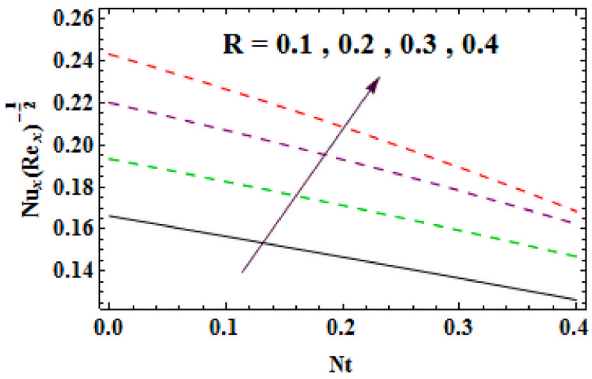

Fig. 24. $Nu_x(\mathrm{Re}_x)^{-\frac{1}{2}}$ versus R and Nt.

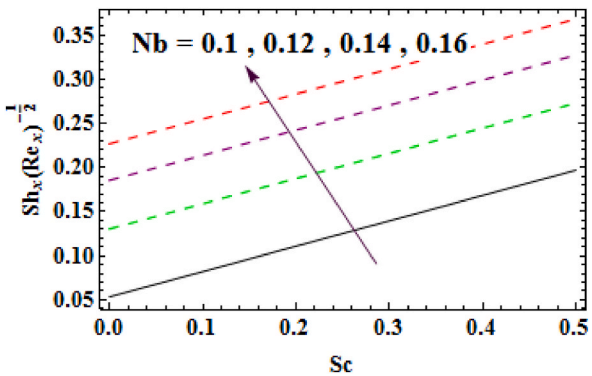

Fig. 25. $Sh_x(\mathrm{Re}_x)^{-\frac{1}{2}}$ versus Nb and Sc.

Fig. 25. It is observed that $Sh_x(\mathrm{Re}_x)^{-\frac{1}{2}}$ rises via higher Nt values. Fig. 26 give $Nn_x(\mathrm{Re}_x)^{-\frac{1}{2}}$ for Pe and Lb.Density number is more for higher Peclet number and Lewis number.

4.6. Entropy generation and Bejan number

Figs. 26 to 33 show influences of Br, M, L and L_1 on N_G and Be. Figs. $(26-27)$ show Br influence on N_G and Be. For higher Br entropy upsurges while Be decreases. Figs. $(28-29)$ give M impact on N_G and Be. For upturn in M entropy escalates while Be decays. Physically resistance inside liquid particles increases for larger M due to which disorder in the system increases so N_G increases. For larger values of M Bejan number decreases as viscous effects are stronger then heat and mass transfer effects. Figs. $(30-31)$ portray influences of L on N_G and Be. For larger L diffusivity in fluid particles rises which enhances disorder in the system as a result N_G

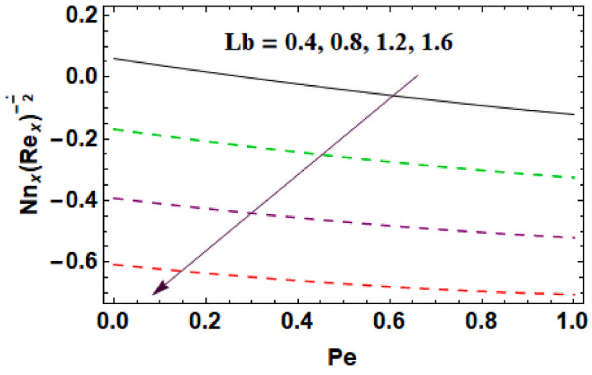

Fig. 26. $Sh_x(\mathrm{Re}_x)^{-\frac{1}{2}}$ versus Lb and Pe.

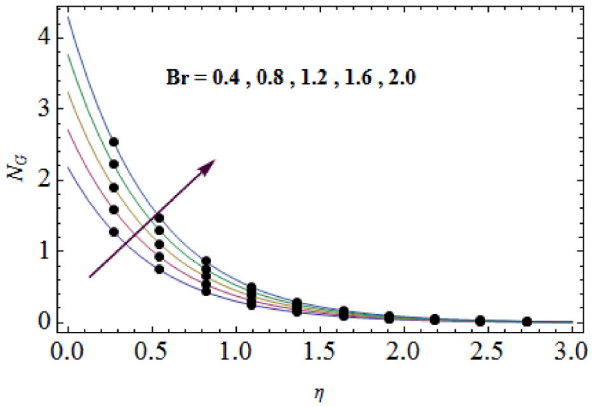

Fig. 27. Br impact on N_G.

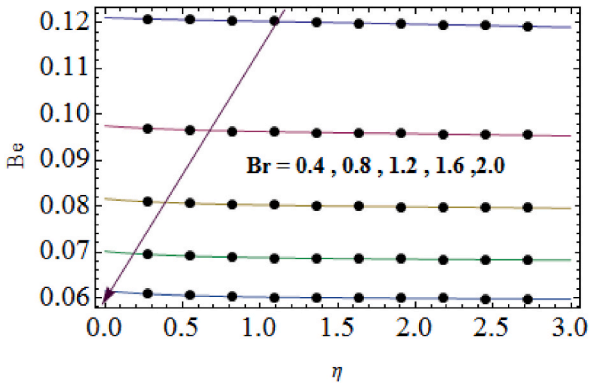

Fig. 28. *Br impact on Be.*

increases and same behavior is observed for Be. In Figs. $(33-34)$ influence of L_1 on N_G and Be is studied. N_G upsurges for enlargement in L_1 while opposite behavior holds for Be.

5. Conclusions

In this study we examined chemically reactive flow of Walter's-B nanofluid in presence of gyrotactic microorganisms accounting the aspects of thermal radiation, heat generation, Darcy-Forchheimer, magnetic field and MHD. HAM code of Mathematica is implemented to tackle the obtained dimensionless highly nonlinear and coupled system. The main conclusions drawn are as follows.

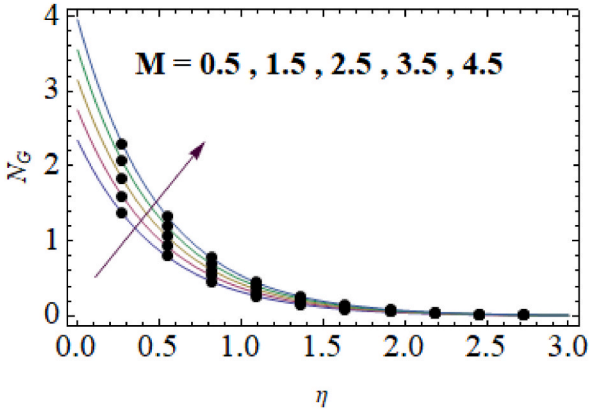

Fig. 29. M impact on N_G.

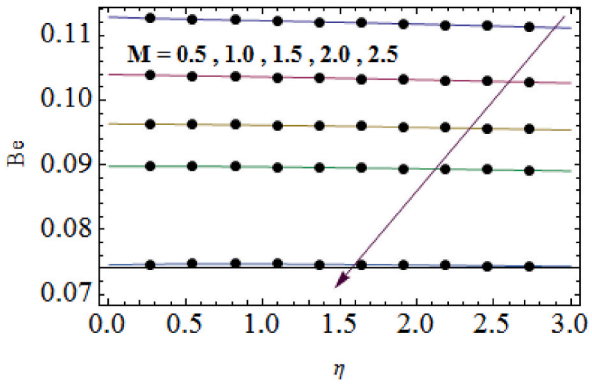

Fig. 30. M impact on Be.

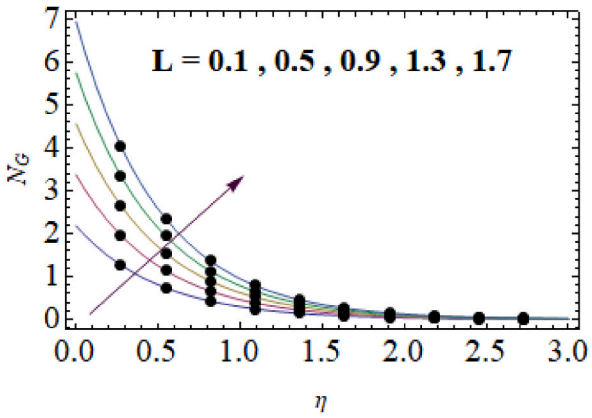

Fig. 31. L impact on N_G.

1 For higher β, Fr, M and λ velocity profile decreases.
2 Temperature profile decreases for higher β and Pr while $\theta(\eta)$ escalates for higher M, Nb, Nt, R and Ec.
3 $\varphi(\eta)$ upsurges for larger Nt, E_1 and δ_1 whereas it decreases for higher γ, Sc and Nb.
4 Motile density decreases versus higher Lb, Pe and Ω.
5 Entropy generation increases for larger values of Br, M, L and L_1.
6 Bejan number upsurges for higher values of L while it decays for higher Br, M and L_1.

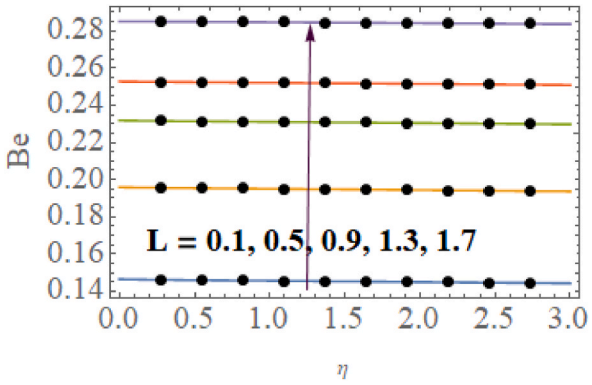

Fig. 32. L impact on Be.

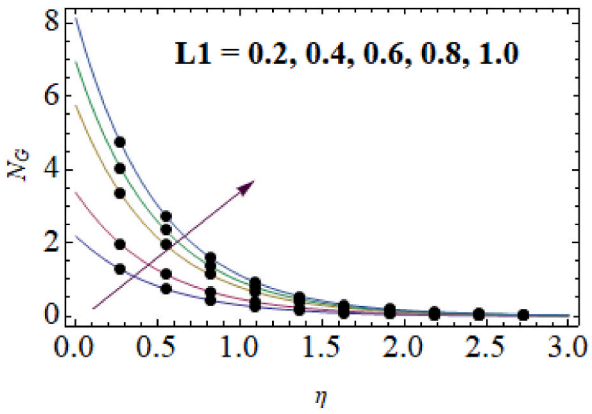

Fig. 33. L_1 impact on N_G.

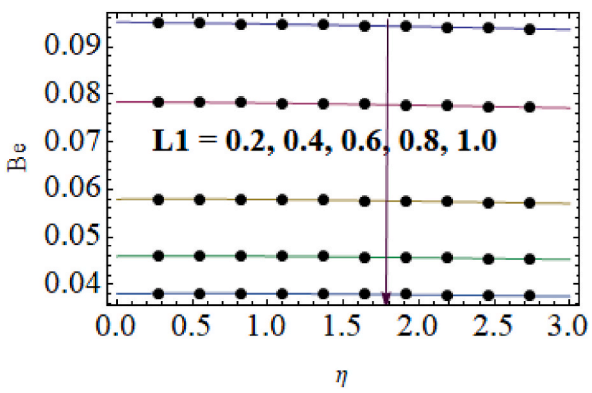

Fig. 34. L_1 impact on Be.

5.1. Future research directions

The main objective of this study was to explore the irreversibility in Walter's-B fluid in presence of gyrotactic microorganisms and nano-sized solid tiny particles. Although this study covers a wide range of aspects regarding modeling and analysis of Walter's-B fluid. However, the following recommendations may be considered for further future research in this context.

- In this study Fourier and Fick's laws for heat and mass transportation are considered, it could be interesting to extend the current study incorporating Cattaneo-Christov heat and mass flux.

- The choice of different geometries, like, three dimensional flows, flows over curved stretching surface, flows in channel; flows over rotating disk may also be future considerations.

Funding

Princess Nourah bint Abdulrahman University Researchers Supporting Project number (PNURSP2023R61), Princess Nourah Bint Abdulrahman University, Riyadh, Saudi Arabia.

Author contribution statement

Mujeeb ur Rahman, Fazal Haq, Pompei C. Darab: Conceived and designed the analysis.
Mohammed Sallah: Analyzed and interpreted the data.
Shaimaa A. M. Abdelmohsen, Basim M. Makhdoum: Contributed analysis tools or data.
Bandar M. Fadhl: Analyzed and interpreted the data; Wrote the paper.

Data availability statement

No data was used for the research described in the article.

Declaration of competing interest

The authors declare that they have no known competing financial interests or personal relationships that could have appeared to influence the work reported in this paper.

Acknowledgments

The authors express their gratitude to Princess Nourah bint Abdulrahman University Researchers Supporting Project number (PNURSP2023R61), Princess Nourah bint Abdulrahman University, Riyadh, Saudi Arabia. This research was partially supported by the project 38 PFE in the frame of the programme PDIPFE-CDI 2021.

Nomenclature

(u, v) components of velocity (ms^{-1}) ρ electric conductivity $(kg^{-1}m^{-3}s^3A^2)$
ν kinematic viscosity (m^2s^{-1}) W_c swimming velocity of maximum cells
B_0 intensity of magnetic field $(kg\,s^{-2}A^{-1})$ F_e inertial coefficient (kgm^2)
k_p porous medium permeability (m^2) C_p specific heat $(Jkg^{-1}K^{-1})$
k thermal conductivity $(Wm^{-1}K^{-1})$ D_B Brownian movement coefficient (m^2s^{-1})
μ fluid friction $(kgm^{-1}s^{-1})$ $\xi(\eta)$ motile density $(-)$
Nn_x density number $(-)$ ρ density of fluid (kgm^{-3})
D_T thermophoresis dispersion coefficient (m^2s^{-1}) n fitted rate constant $(-)$
k^* mean absorption coefficient (m^{-1}) k_r^2 chemical reaction rate (s^{-1})
T temperature (K) Ea activation energy coefficient $(kg\,m^2\,s^{-2})$
σ^* Stefan Boltzmann constant $(Js^{-1}m^{-2}\,K^{-4})$ T_∞ ambient temperature (K)
η dimensionless variable $(-)$ C concentration $(-)$
τ heat capacity ratio $(-)$ b chemotaxis constant (m)
μ fluid friction $(kgm^{-1}s^{-1})$ κ Boltzmann constant (eVK^{-1})
Q_0 heat generation coefficient $(W\,m^{-2}K^{-1})$ N concentration of microorganisms $(-)$
C_∞ ambient concentration $(-)$ $u_w(x)$ stretching rate (ms^{-1})
D_m microorganisms diffusivity coefficient (m^2s^{-1}) q_w heat flux (Js^{-2})
β viscoelastic parameter $(-)$ M magnetic variable $(-)$
λ porosity parameter $(-)$ Sh_x Sherwood number $(-)$
Fr Forchheimer variable $(-)$ $\theta(\eta)$ temperature $(-)$
τ_w shear stress (Wm^{-2}) R radiation variable $(-)$
$\varphi(\eta)$ concentration $(-)$ Pr Prandtl variable $(-)$
J_w mass flux (ms^{-1}) Nb Brownian movement variable $(-)$
Fr Forchheimer variable $(-)$ E_1 activation energy parameter $(-)$
Ec Eckert number $(-)$ Lb bioconvection Lewis number $(-)$
Sc Schmidt number $(-)$ δ_1 temperature difference ratio variable $(-)$
Nt thermophoresis diffusion variable $(-)$ ξ motile density of microorganisms $(-)$

γ chemical reaction variable (–) Q injection parameter (–)
Ω microorganisms difference ratio variable (–) Cf wall shear force (–)
Pe bioconvection Peclet number (–) Nu_x Nusselt number (–)

References

[1] T. Hayat, M.I. Khan, M. Farooq, A. Alsaedi, M. Waqas, T. Yasmeen, Impact of Cattaneo-Christov heat flux model in flow of variable thermal conductivity fluid over a variable thicked surface, Int. J. Heat Mass Tran. 99 (2016) 702–710.
[2] M.I. Khan, M. Waqas, T. Hayat, A. Alsaedi, A comparative study of Casson fluid with homogeneous-heterogeneous reactions, J. Colloid Interface Sci. 498 (2017) 85–90.
[3] U. Adnan, Khan N. Ahmed, S.T. Mohyud-Din, Thermo-diffusion and diffusion thermo effects on flow of second grade fluid between two inclined plane walls, J. Mol. Liq. 224 (2016) 1074–1082.
[4] K.L. Hsiao, Heat and mass transfer for micropolar flow with radiation effect past a nonlinearly stretching sheet, Heat Mass Tran. 46 (2010) 413–419.
[5] M.I. Khan, F. Alzahrani, A. Hobiny, Z. Ali, Fully developed second order velocity slip Darcy-Forchheimer flow by a variable thicked surface of disk with entropy generation, Int. Commun. Heat Mass Tran. 117 (2020), 104778.
[6] S. Nadeem, R. Mehmood, S.S. Motsa, Numerical investigation on MHD oblique flow of Walter's B type nanofluid over a convective surface, Int. J. Therm. Sci. 92 (2015) 162–172.
[7] T. Hayat, S. Asad, M. Mustafa, H.H. Alsulami, Heat transfer analysis in the flow of Walters' B fluid with a convective boundary condition, Chin. Phys. B 23 (2014), 084701.
[8] T.B. Chang, A. Mehmood, O.A. Beg, M. Narahari, M.N. Islam, F. Ameen, Numerical study of transient free convective mass transfer in a Walters-B viscoelastic flow with wall suction, Commu. Nonlinear Sci. Numer. Simul. 16 (2011) 216–225.
[9] T. Hayat, M. Awais, S. Asghar, Radiative effects in a three-dimensional flow of MHD Eyring-Powell fluid, J. Egyp. Math. Soc. 21 (2013) 379–384.
[10] K. Ramesh, M. Devakar, Effect of heat transfer on the peristaltic flow of Walter-B fluid in a vertical channel with external magnetic field, J. Aerospace Eng. 10 (2015), 04015050.
[11] A.M. Alsharif, A.I.Y. Elmaboud, S.I. Abdelsalam, Performance enhancement of a DC-operated micropump with electroosmosis in a hybrid nanofluid: fractional Cattaneo heat flux problem, Appl. Math. Mech. 43 (6) (2022) 931–944.
[12] M.M. Bhatti, S. Abdelsalam, Scientific Breakdown of a Ferromagnetic Nanofluid in Hemodynamics: Enhanced Therapeutic Approach, 17, 2022, p. 44.
[13] M. Kumar, P.K. Mondal, Radiative and hydromagnetic heat transfer analysis of a reiner, –Philippoff Fluid. 37 (1) (2023) 213–226.
[14] A. Mukherjee, P.K. Mondal, Analysis of heat transfer through optically participating medium in a concentric spherical enclosure: the role of dual-phase-lag conduction and radiation, J. Therm. Sci. Eng. Appl. 10 (4) (2018) 17–1455.
[15] M. Ziaei-Rad, M. Saeedan, E. Afshari, Simulation and prediction of MHD dissipative nanofluid flow on a permeable stretching surface using artificial neural network, Appl. Therm. Eng. 99 (2016) 373–382.
[16] R.S. Varun Kumar, A. Alhadhrami, R.J. Punith Gowda, R. Naveen Kumar, B.C. Prasannakumara, Exploration of Arrhenius Activation Energy on Hybrid Nanofluid Flow over a Curved Stretchable Surface, 2021, e202100035.
[17] M.I. Khan, Transportation of hybrid nanoparticles in forced convective Darcy–Forchheimer flow by a rotating disk, Int. Commun. Heat Mass Tran. 122 (2021), 105177.
[18] H. Xu, I. Pop, Fully developed mixed convection flow in a horizontal channel filled by a nanofluid containing both nanoparticles and gyrotactic microorganisms, Eur. J. Mech. B Fluid 46 (2014) 337–345.
[19] L. Tham, R. Nazar, I. Pop, Mixed convection flow over a solid sphere embedded in a porous medium filled by ananofluid containing gyrotactic microorganisms, Int. J. Heat Mass Tran. 62 (2013) 647–660.
[20] A. Ali, S. Sarkar, S. Das, Physical Insight into Magneto-Thermo-Migration of Motile Gyrotactic Microorganisms over a Flexible Cylinder with Wall Slip, and Arrhenius Kinetics, Waves in Random and Complex Media, 2023, pp. 1–24, https://doi.org/10.1080/17455030.2023.2178059.
[21] A. Aziz, W.A. Khan, I. Pop, Free convection boundary layer flow past a horizontal flat plate embedded in porous medium filled by nanofluid containing gyrotactic microorganisms, Int. J. Therm. Sci. 56 (2012) 48–57.
[22] S. Sarkar, A. Ali, S. Das, Bioconvection in non-Newtonian nanofluid near a perforated Riga plate induced by haphazard motion of nanoparticles and gyrotactic microorganisms in the attendance of thermal radiation, and Arrhenius chemical reaction: sensitivity analysis, Int. J. Ambient Energy 43 (2022) 1–34.
[23] N.S. Akbar, Z.H. Khan, Magnetic field analysis in a suspension of gyrotactic microorganisms and nanoparticles over a stretching surface, J. Magn. Magn Mater. 410 (2016) 72–80.
[24] W.N. Mutuku, O.D. Makinde, Hydromagnetic bioconvection of nanofluid over a permeable vertical plate due to gyrotactic microorganisms, Comput. Fluid 95 (2014) 88–97.
[25] A.V. Kuznetsov, A.A. Avramenko, Effect of small particles on the stability of bio convection in a suspension of gyrotactic microorganisms in a layer of finite depth, Int. Commun. Heat Mass Tran. 31 (2004) 1–10.
[26] S. Sarkar, T.K. Pal, A. Ali, S. Das, Themo-bioconvection of gyrotactic microorganisms in a polymer solution near a perforated Riga plate immersed in a DF medium involving heat radiation, and Arrhenius kinetics, Chem. Phys. Lett. 797 (2022), 139557.
[27] A. Bejan, A study of entropy generation in fundamental convective heat transfer, J. Heat Tran. 101 (1979) 718–725.
[28] M.I. Khan, S. Qayyum, T. Hayat, A. Alsaedi, M.I. Khan, Investigation of Sisko fluid through entropy generation, J. Mol. Liq. 257 (2018) 155–163.
[29] V.S. Ramesh, D. Reddy, M.G. Azese, S. Abdelsalam, On the entropy optimization of hemodynamic peristaltic pumping of a nanofluid with geometry effects, in: Waves in Random and Complex Media, 2022, https://doi.org/10.1080/17455030.2022.2061747.
[30] A. Gul, I. Khan, S.S. Makhanov, Entropy generation in a mixed convection Poiseulle flow of molybdenum disulphide Jeffrey nanofluid, Results Phys. 9 (2018) 947–954.
[31] Z.Y. Xie, Y.J. Jian, Entropy generation of two-layer magnetohydrodynamic electroosmotic flow through microparallel channels, Energy 139 (2017) 1080–1093.
[32] M.I. Khan, S. Ullah, T. Hayat, M.I. Khan, A. Alsaedi, Entropy generation minimization (EGM) for convection nanomaterial flow with nonlinear radiative heat flux, J. Mol. Liq. 260 (2018) 279–291.
[33] R.J. Punith Gowda, R. Naveen Kumar, A.M. Jyothi, B.C. Prasannakumara, K.S. Nisar, KKL Correlation for Simulation of Nanofluid Flow over a Stretching Sheet Considering Magnetic Dipole and Chemical Reaction, 2021, e202000372.
[34] G. Huminic, A. Huminic, The heat transfer performances and entropy generation analysis of hybrid nanofluids in a flattened tube, Int. J. Heat Mass Tran. 119 (2018) 813–827.
[35] T. Hayat, M. Rafiq, B. Ahmad, S. Asghar, Entropy generation analysis for peristaltic flow of nanoparticles in a rotating frame, Int. J. Heat Mass Tran. 108 (2017) 1775–1786.
[36] D. Nouri, M. Pasandideh-Fard, M.J. Oboodi, O. Mahian, A.Z. Sahin, Entropy generation analysis of nanofluid flow over a spherical heat source inside a channel with sudden expansion and contraction, Int. J. Heat Mass Tran. 116 (2018) 1036–1043.
[37] M. Vatanmakan, E. Lakzian, M.R. Mahpeykar, Investigating the entropy generation in condensing steam flow in turbine blades with volumetric heating, Energy 147 (2018) 701–714.
[38] H.S. Gaikwad, P.K. Mondal, S. Wongwises, Non-linear drag induced entropy generation analysis in a microporous channel: the effect of conjugate heat transfer, Int. J. Heat Mass Tran. 108 (2017) 2217–2228.

[39] R. Sarma, A.K. Shukla, H.S. Gaikwad, P.K. Mondal, S. Wongwises, Effect of conjugate heat transfer on the thermo-electro-hydrodynamics of nanofluids: entropy optimization analysis, Journal of Thermal Analysis and Calorimetry 147 (1) (2022) 599–614.
[40] S. Li, F. Ali, A. Zaib, K. Loganathan, S.M. Eldin, M.I. Khan, Bioconvection effect in the Carreau nanofluid with Cattaneo–Christov heat flux using stagnation point flow in the entropy generation: micromachines level study, Open Phys. 21 (2023), 20220228.
[41] Z. Dai, Z. Ma, X. Zhang, J. Chen, R. Ershadnia, X. Luan, M.R. Soltanian, An integrated experimental design framework for optimizing solute transport monitoring locations in heterogeneous sedimentary media, J. Hydrol. 614 (2022), 128541, https://doi.org/10.1016/j.jhydrol.2022.128541.
[42] S. Li, M.I. Khan, F. Alzahrani, S.M. Eldin, Heat and mass transport analysis in radiative time dependent flow in the presence of Ohmic heating and chemical reaction, viscous dissipation: an entropy modeling, Case Stud. Therm. Eng. 42 (2023), 102722.
[43] M. Qu, T. Liang, J. Hou, Z. Liu, E. Yang, X. Liu, Laboratory study and field application of amphiphilic molybdenum disulfide nanosheets for enhanced oil recovery, J. Petrol. Sci. Eng. 208 (2022), 109695, https://doi.org/10.1016/j.petrol.2021.109695.
[44] X. Zhang, X. Sun, T. Lv, L. Weng, M. Chi, J. Shi, S. Zhang, Preparation of PI porous fiber membrane for recovering oil-paper insulation structure, J. Mater. Sci. Mater. Electron. 31 (16) (2020) 13344–13351, https://doi.org/10.1007/s10854-020-03888-5.
[45] L. Zhang, J. Zhang, X. Wang, M. Tao, G. Dai, J. Wu, X. Lin, Design of coherent wideband radiation process in a Nd3+-doped high entropy glass system, Light Sci. Appl. 11 (1) (2022) 181, https://doi.org/10.1038/s41377-022-00848-y.
[46] W. Liu, C. Zhao, Y. Zhou, X. Xu, R.A. Rakkesh, Modeling of vapor-liquid equilibrium for electrolyte solutions based on COSMO-RS interaction, J. Chem. 2022 (2022), 9070055, https://doi.org/10.1155/2022/9070055.
[47] X. Li, Z. Dong, L. Wang, X. Niu, H. Yamaguchi, D. Li, P. Yu, A magnetic field coupling fractional step lattice Boltzmann model for the complex interfacial behavior in magnetic multiphase flows, Appl. Math. Model. 117 (2023) 219–250, https://doi.org/10.1016/j.apm.2022.12.025.
[48] Z.N. Wu, L. Lin, Nanofluidics for single-cell analysis, Chin. Chem. Lett. 33 (4) (2022) 1752–1756.
[49] W. Xiang, et al., Amplification effects of magnetic field on hydroxylamine-promoted ZVI/H2O2 near-neutral Fenton like system, Chin. Chem. Lett. 33 (3) (2022) 1275–1278.
[50] C.Y. Wang, Free convection on a vertical stretching surface, J. Appl. Math. Mech. 69 (1989) 418–420.
[51] W.A. Khan, I. Pop, Boundary-layer flow of a nanofluid past a stretching sheet, Int. J. Heat Mass Tran. 53 (2010) 2477.